Power Transfer With an Inductive Link and Wireless Tuning

ARTICLE *in* IEEE TRANSACTIONS ON INSTRUMENTATION AND MEASUREMENT · MAY 2013

Impact Factor: 1.79 · DOI: 10.1109/TIM.2013.2245041

Power Transfer With an Inductive Link and Wireless Tuning

Valner J. Brusamarello, *Member, IEEE*, Yeddo Braga Blauth, Ricardo de Azambuja , *Student Member, IEEE*, Ivan Muller, *Student Member, IEEE*, and Fernando Rangel de Sousa, *Member, IEEE*

***Abstract*—This paper presents the analysis of two air-coupled coils used to transfer energy to charge a battery. This battery is used to power an electronic device designed to monitor variables such as impact strength, range of temperature, and humidity associated with the transport of fruits. The device is inside a sealed enclosure that cannot be opened for recharging the battery. The study shows that the coupled coils need to work with a resonance capacitor, at least on the secondary coil. However, the resonance frequency also depends on the coupling factor k. Therefore, this work proposes a monitoring system with a closed loop for fine-tuning the resonance frequency of the secondary coil circuit. Before starting charging the battery, the system scans the resonance frequency on the primary coil and measures the output power on the secondary coil looking for the optimal point. This procedure reduces problems of coupling factor variations with positioning of the coils during the battery charging.**

***Index Terms*—Air-coupled coils, battery charging, resonance, wireless.**

I. Introduction

MAGNETICALLY coupled coils have been widely used for a variety of applications requiring contactless or wireless power such as biomedical devices [1], [2] and instrumentation systems [3], among others [4]–[6]. In such applications, the energy transfer from the source to the load is done by loosely coupled coils. These coils can be represented by the primary and secondary inductances L_1 and L_2, with a low coupling coefficient k_{12}.

In order to enhance the power transfer capability, the loosely coupled coils generally need to be compensated with capacitors to obtain the resonance effect [1]–[7]. In addition to the power transfer capability, the operating efficiency of the coupled coils is of concern to many applications [7]. In fact, applications such as biomedical implanted devices [1], [2] may require efficient power transfer in order to reduce the time of charging associated to uncomfortable positions and to avoid exposing the body tissue to high intensity fields [8]. In other applications the efficiency of the inductive link is required in order to avoid energy wasting, such as automotive battery charging devices [5]. The link efficiency mostly depends on three factors, the coil losses, coupling factor, and impedance matching [8]. The inductive power transfer system suffers severely from inefficient operation, particularly under light loading conditions [9]. Usually, in order to achieve the maximal power transfer efficiency, some tuning technique is applied to the circuit. A typical approach for controlling the system uses variable-frequency control in the resonant inverter to meet the zero phase angle in the load impedance and uses pulsewidth-modulation technique in the controlled rectifier of the output side to control the output voltage or current [5].

According to the authors of [2], [10], and [11], the power flow control of wireless power pickups is an important point to further developments in controlled power transfer in such devices. Load variations, magnetic coupling variations between the coils, and operating frequency drifting can cause the output voltage of the secondary power pickup to deviate significantly from the original designed value, resulting in an undesirable characteristic in applications where a constant and stable output voltage is required [10]–[14]. Different methods have been proposed for controlling the load in loosely coupled coils such as the shorting control method [14] or the dynamic tuning/detuning technique proposed in [5], [15], and [16]. The fundamental concept of the last technique is to dynamically change the tuning condition of the power pickup according to the actual load requirements.

Nowadays, there is an increasing development of wireless devices, which need battery recharging regularly. Coreless transformers have been proposed to work as the charger to wireless devices such as mobile phones, where the primary core of the transformer is in the charger unit and the secondary core is in the phone [4]. To simplify coil manufacture, printed circuit boards were used instead of usual windings [17]. In another application, a detachable transformer is presented as a noncontact charging system for the batteries of an electrical shaver using a resonant converter [18].

This paper describes the study of an inductive power transfer system for charging the batteries of an instrument that mimes a fruit such as an apple or an orange (pseudofruit). Among other important variables, the device records the mechanical shocks, using a three-ring load cell during the postharvest processing of apples and oranges [19], [20]. The small signals are acquired by a digital system and sent through a radio channel, which is linked to a host device. In this paper, the same radio link is used

Manuscript received July 1, 2012; revised August 26, 2012; accepted September 24, 2012. Date of publication March 20, 2013; date of current version April 3, 2013. The Associate Editor coordinating the review process for this paper was Dr. Kurt Barbe.

V. J. Brusamarello, Y. B. Blauth, R. de Azambuja, and I. Muller are with the Electrical Engineering Department, Universidade Federal do Rio Grande do Sul, 90040-060 Porto Alegre RS, Brazil (e-mail: valner.brusamarello@ufrgs.br; yeddo@ufrgs.br; ricardo.azambuja@ieee.org; ivan.muller@ufrgs.br).

F. R. de Sousa is with the Electrical Engineering Department, Universidade Federal de Santa Catarina, 88040-970 Florianópolis SC, Brazil (e-mail: rangel@ieee.org).

Color versions of one or more of the figures in this paper are available online at http://ieeexplore.ieee.org.

Digital Object Identifier 10.1109/TIM.2013.2245041

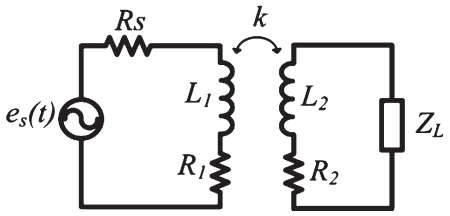

Fig. 1. Two circuit for wireless energy transferring.

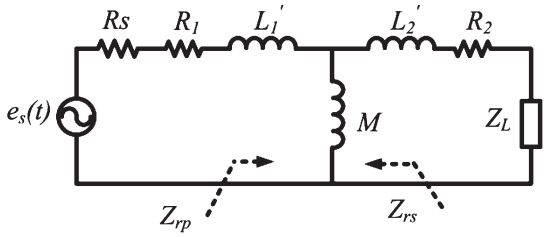

Fig. 2. Equivalent circuit.

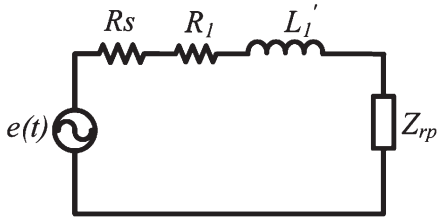

Fig. 3. Total impedance on the primary side of the inductive link.

to carry the data signal of voltage and current delivered by the secondary side of the inductive link during the battery charging. Thus, the power transfer operates as a closed-loop system. The digital system in the device monitors the data signals and communicates to the base, which starts a scan for the tune frequency point, featuring a wireless loop control strategy. The following sections will show how important and sensible to small changes is the tune frequency to the maximum power delivered from the secondary coil to the load, as well as the maximum efficiency. With these features, the pseudofruit can be made watertight, a desirable characteristic for deployment in harsh places such as water-based fruit selection machines and bulk transportation.

In a previous work [21], the results of an analytical study of the inductive power transfer between two coils, which is based on a resonant circuit, showed that the resonance frequency depends directly on the coupling factor k. In this paper, we have developed a prototype of an inductive link and present the results of the change in alignment of the two coils in terms of the inductive coupling factor k, the variation of resonance frequency, the variation of power transferred from the link to the load, and the variation of the efficiency of the system. The misalignment of the coils is evaluated in three distinct relative positions between the primary and secondary coils. The chosen relative positions represent the case where the secondary and primary coils are aligned, with $k = 0.6$, the case where the coils present a misalignment of around 30° with $k = 0.3$ (worst case), and a third situation between the limits of the previous cases, representing a $k = 0.4$.

The results showed that a correct choice of parameters, together with the control of the excitation frequency, can optimize efficiency and maximum power transfer to the load.

II. Circuit Analysis

A. Analysis of the Primary Coil

Fig. 1 shows a basic wireless power transferring circuit composed of a pair of inductively coupled coils L_1 (primary) and L_2 (secondary). The energy is supplied by the voltage source $e_S(t)$ and is delivered by the link to the load Z_L. R_S is the supply voltage internal resistance, and R_1 and R_2 are the losses of the primary and secondary coils, respectively. The intensity of the coupling between L_1 and L_2 is measured by the coupling factor k, given by

$$k = \frac{M}{\sqrt{L_1 L_2}} \tag{1}$$

where M is the mutual inductance between L_1 and L_2.

The three important aspects of the circuit of Fig. 1 are as follows: 1) the link efficiency; 2) the maximum amount of power delivered to the link; and 3) the maximum power delivered from the link to the load. The first is dependent on the coil losses, coupling factor, and frequency, while the second is a function of the matching between the source internal resistance and equivalent impedance on the primary side of the link. The third aspect depends on the matching between the load and the secondary equivalent impedance.

The equivalent impedance presented to the supply voltage can be found by analyzing the circuit of Fig. 2, which is an equivalent model [22] of the link shown in Fig. 1. In the model, $e_S(t) = E\cos(\omega t)$, $L_1' = L_1 - M$, $L_2' = L_2 - M$, and $Z_L = R_L + jX_L$. The reflected impedance on the primary side is given by

$$Z_{rp} = \frac{(R_L+R_2)(\omega M)^2}{(R_L+R_2)^2+(X_L+\omega L_2'+\omega M)^2} + \frac{j\omega M\left[(R_L+R_2)^2+(X_L+\omega L_2')\left(X_L+\omega L_2'+\omega M\right)\right]}{(R_L+R_2)^2+(X_L+\omega L_2'+\omega M)^2}. \tag{2}$$

Combining (2) with R_1 and L_1', we have the total impedance presented to the power source (see Fig. 3)

$$Z_p = R_1 + j\omega L_1' + Z_{rp}. \tag{3}$$

The current supplied by the power source is dependent on its internal resistance R_S and the total primary side impedance defined by (3). From (3), we can also calculate the capacitor necessary to cancel the reactive equivalent impedance of the link. For example, supposing that the load is purely resistive ($X_L = 0$), the series resonating capacitor can be calculated by

$$C_1 = \frac{1}{\omega^2\left[L_1' + \frac{M\left[(R_2+R_L)^2+\omega^2 L_2'\left(L_2'+M\right)\right]}{(R_2+R_L)^2+\omega^2\left(L_2'+M\right)^2}\right]}. \tag{4}$$

The reactance $X_M = \omega M$ depends on the primary and secondary inductance coils. This reactance also depends on the

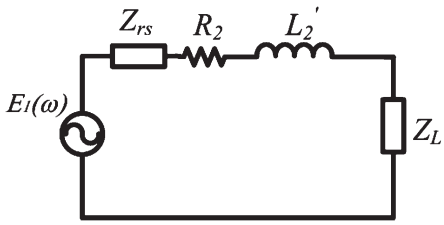

Fig. 4. Equivalent circuit on the secondary side of the inductive link.

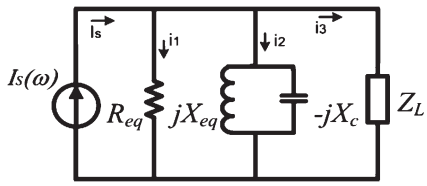

Fig. 5. Equivalent source supplying the current to the load on the resonance.

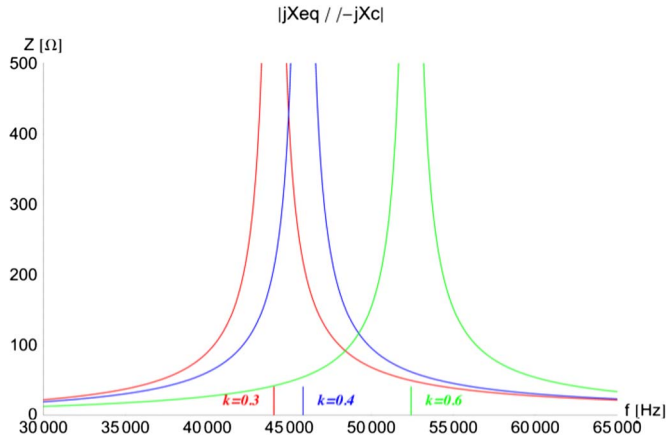

Fig. 6. Resulting impedance of the parallel association between the equivalent inductance and the compensation capacitor (from Fig. 5) for several values of coupling factors k.

coupling constant k, which changes with the relative position of both coils. The variation of mutual inductance is reflected on the inductance of both sides, primary and secondary, and thus, it also influences the resonance frequency of the circuit.

B. Analysis of the Secondary Coil

Considering the primary coil connected to a sinusoidal wave source and the secondary connected to a load, one can calculate the equivalent circuit from the load side (see Fig. 2). The voltage reflected on the secondary coil $E_1(\omega)$ is defined by

$$E_1(\omega) = E(\omega)\frac{(X_{L1}X_M + jX_M R_1)}{R_{T1}^2 + X_1^2}. \quad (5)$$

Where $E(\omega)$ is the sinusoidal voltage source $e_s(t)$ on the frequency domain and $R_{T1} = R_1 + R_S$. Finally, the equivalent impedance reflected on the secondary coil is

$$Z_{rs} = \frac{X_M^2 R_{T1} + j\left(X_M X_{L1}^2 - X_M^2 X_{L1} + X_M R_{T1}^2\right)}{R_{T1}^2 + X_{L1}^2}. \quad (6)$$

The equivalent circuit on the secondary coil of the inductive link is shown in Fig. 4.

C. Resonance Effect on the Secondary Coil

In the circuit of Fig. 4, the power transfer capability is enhanced by connecting a capacitor in parallel to the load in order to reach the resonance. The equivalent parallel circuit of Fig. 5 shows the capacitor, an equivalent inductance, and an equivalent resistance. The equivalent current source $I_S(\omega)$ is defined by

$$I_S(\omega) = \frac{E(\omega)\frac{(X_{L1}X_M + jX_M R_1)}{R_1^2 + X_{L1}^2}}{R_{L2} + j(X_{L2} - X_M) + Z_{\mathrm{Ref}2}}. \quad (7)$$

The resistor R_{eq} represents the effects of the internal resistance of the input voltage source reflected to secondary side, the intrinsic resistances of the inductors reflected to the secondary side, and the intrinsic resistance of the resonant capacitor. In this equivalent circuit, when the resonance frequency of the tank circuit equals the frequency of the equivalent current source, the net current i_2 is zero. In that situation, the current from the source is divided by the load (current i_3) and the equivalent resistance R_{eq} (current i_1). One should notice that, in the real situation, the intrinsic resistances cannot be separated from the inductor and the capacitor. In this model, if the equivalent resistance R_{eq} is high enough, then i_1 tends to zero and most of the current I_s is supplied to the load.

If the load is resistive, the resonant capacitor value is a function of the circuit frequency and the circuit components. One can notice that, in the resonant frequency, the maximum power transferred by this circuit to the load occurs when the equivalent resistance (of the equivalent circuit) is equal to the load resistance. Variations in the capacitance or in the inductance of this circuit can detune the resonance. Also, the equivalent inductance of the circuit from Fig. 4 depends on the coupling factor k, which depends on the geometric position of both coils. Each time that the coils are moved, they present a different coupling factor, resulting in a variable mutual inductance. Moreover, environmental factors such as humidity and temperature variations can change the capacitor value. Both situations require to fine-tune the resonance point of the circuit.

The dependence of the circuit's resonance frequency on the coupling factor can be seen in Fig. 6. The values of the coupling factor k used in this work are based on measurements of a prototype coil, which are presented in the next sections.

The resulting impedance of the parallel association between the equivalent inductance in the secondary coil and the compensation capacitor (from Fig. 5) is illustrated in Fig. 6 for a few values of the coupling factor k. This range was chosen since these values are close to those obtained in the application scenario. The equivalent impedance of Fig. 6 has an important influence on the equivalent voltage (Thévenin voltage) in the load as shown in Fig. 7. One can notice that low coupling factors do not considerably affect the resonance frequency of the circuit. Moreover, one can figure out that the resonance frequency is especially sensitive to high values of k since it is dependent on the mutual inductance defined by (1), as can be noticed by the mutual reactance X_M in (6).

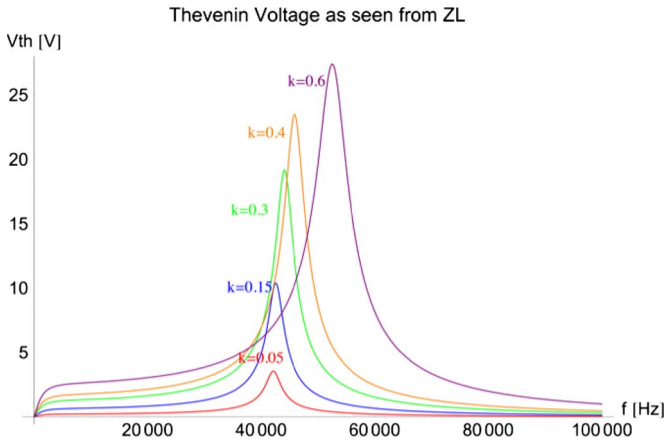

Fig. 7. Dependence of the resonance frequency on the coupling factor k.

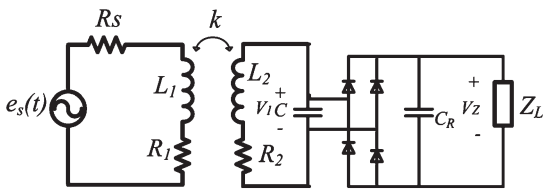

Fig. 8. Simulated circuit used to analyze the nonlinear load.

D. Nonlinear Load

A rectifier circuit is necessary in order to employ a wireless power transfer system in applications such as battery chargers. The diode bridge connected to the battery features a nonlinear load. The analysis of this circuit (see Fig. 8) was first made with a simulator based on SPICE. Considering the capacitor C_R large enough to maintain the voltage V_Z almost constant, the circuit of the battery charger can be considered a resistor. In these simulations, the load Z_L is a resistor, which assumes different values. The capacitor C is calculated in order for the secondary circuit to reach the resonance frequency at about 50 kHz. The results of the simulations are summarized in Table I. The circuit parameters are $R_S + R_1 = 1\ \Omega$, $R_2 = 0.9\ \Omega$, $L_1 = 90\ \mu$H, $L_2 = 68\ \mu$H, $C = 210$ nF, and $C_R = 100\ \mu$F. $e_s(t)$ is an ac pulse source ranging from -5 to $+5$ V. The frequency is fixed for each k.

Although the load is composed by a rectifier circuit, it is usual to represent this load with an equivalent resistance [23], [24]. A battery is usually represented by a model consisting of capacitors and resistors. However, in our context, the process is slow, and the current always has a positive direction. Thus, we can consider, for the purpose of simplified analysis, the battery as a resistance.

Thus, we assume the load Z_L in Fig. 8 to be a set of resistors, and Table I shows some results. One can notice that the maximum power, for this particular case of parameters, occurs when the load takes a value around 270 Ω. The value of load resistance strongly influences the output dc voltage. In the case of the battery charger, this indicates the need for a dc–dc converter to adapt the circuit voltage V_Z to the battery voltage. The simulation results also show the dependence of the resonant frequency on the coupling factor k and the low efficiency on low values of load. Fig. 9 illustrates the dependence of the power for different values of load resistance (fixed coupling factor $k = 0.3$). One can notice the maximum power transfer to the load ($R_L \cong 186\ \Omega$) and the resonance frequency ($f \cong 45$ kHz).

Fig. 10 illustrates the power on the load versus the frequency and the coupling factor k.

TABLE I
VOLTAGE ON THE LOAD BASED ON SIMULATED VALUES

	Z_L	$V_1\,(AC)$	$V_Z\,(DC)$	η (%)
k=0.3 43kHz	6.8Ω	2.3 Vp	0.3 V	5
	47 Ω	3.3 Vp	1.5 V	27
	270 Ω	8.2 Vp	6 V	74
	470 Ω	10.5 Vp	8.1 V	65
	1k Ω	13.4 Vp	10.8 V	50
k=0.4 46kHz	6.8Ω	2.2 Vp	0.3 V	6
	47 Ω	4.0 Vp	2.0 V	32
	270 Ω	9.9 Vp	7.6 V	61
	470 Ω	11.5 Vp	9.5 V	48
	1k Ω	13.4 Vp	11.6 V	30
k=0.6 52kHz	6,8Ω	2.5 Vp	0.6 V	11
	47 Ω	5.7 Vp	3.5 V	47
	270 Ω	13.9 Vp	11.7 V	55
	470 Ω	16.8 Vp	14.6 V	40
	1k Ω	19.4 Vp	17.6 V	23

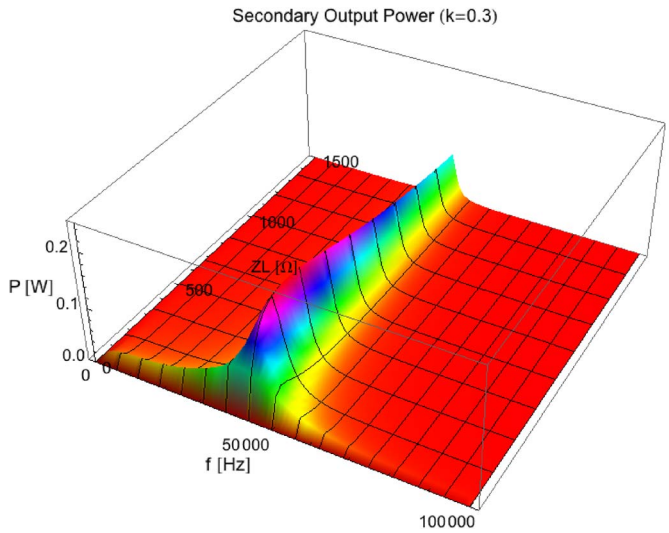

Fig. 9. Power delivered to the load, P, as a function of the frequency and load resistance for $k = 0.3$.

E. Efficiency Analysis

Since one of the objectives of this work, and its application, is to increase the power in the load using the effects of resonance, the efficiency of the link is also of great importance. In order to study the tuning effects on the efficiency of the inductive link,

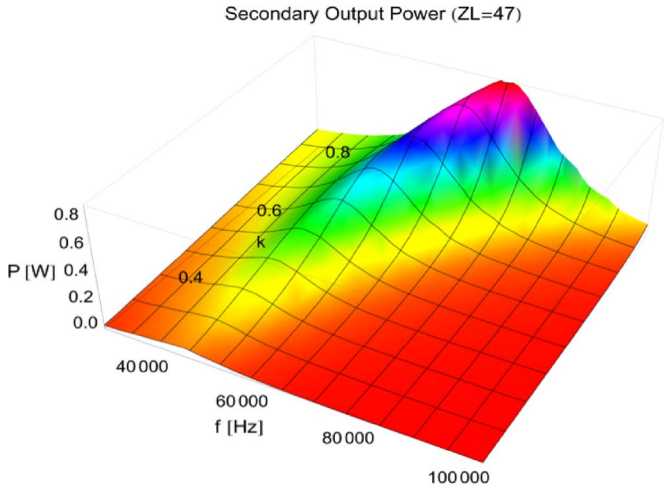

Fig. 10. Dependence of power transferred on the variation of the frequency for a range of values of coupling factor k.

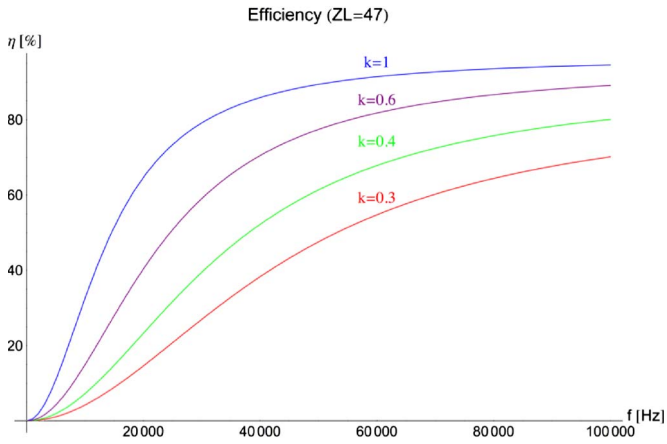

Fig. 11. Dependence of efficiency (circuit of Fig. 2) on the variation of the frequency for some values of the coupling factor k when the load is 47 Ω.

one should start with a simple circuit without compensation (see Fig. 2). The link efficiency can be defined as the ratio between the power delivered to the load and the power delivered by the source. After some manipulation, the efficiency of the equivalent circuit of Fig. 2 can be described by

$$\eta = \frac{1}{1 + \frac{L_2(R_1+R_S)}{K^2 L_1 R_L} + \frac{2(R_1+R_S)+X_L}{k^2 L_1 R_L \omega} + \frac{((R_1+R_S)(R_2+R_L)^2+x}{k^2 L_1 L_2 R_L \omega^2}}. \tag{8}$$

Fig. 11 illustrates the efficiency dependence on the coupling factor k and on the frequency ω.

Clearly, this figure shows that, without the presence of the compensation capacitor, the highest efficiency is achieved when the ω value is ∞.

After adding a compensating capacitor in parallel with the load Z_L, as depicted in the equivalent circuit of Fig. 4, the

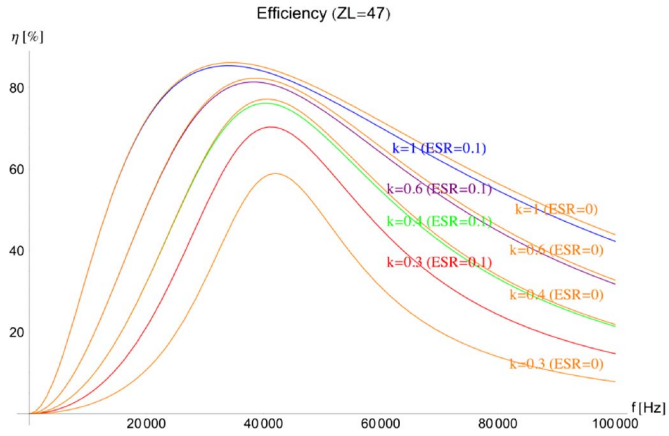

Fig. 12. Dependence of efficiency (circuit of Fig. 4) on the variation of the frequency for values of the coupling factor k.

efficiency equation becomes very complex. However, making some simplifications such as the capacitor $ESR = 0$, the efficiency equation simplifies to

$$\eta = \frac{1}{1 + C_2^2 R_2 R_L \omega^2 + p + \frac{R_2}{R_L}} \tag{9}$$

where p is an expression defined by (10), shown at the bottom of the page.

By analyzing (9) and plotting again the efficiency versus frequency for several coupling factors, there is a $\omega < \infty$ where efficiency is maximal. Fig. 12 illustrates the dependence of the efficiency on the variation of some coupling factors k. In Fig. 12, a set of curves was plotted with capacitor $ESR = 0.1$, and another set of curves was plotted with $ESR = 0$. One can notice that the maximum efficiency does not necessarily occur exactly at the same frequency that the power is maximum in the load.

III. Methodology and Results

The main objective of this work is to study and develop a wireless battery charger to be used in an electronic device designed to monitor variables associated with the transport of fruits. The results of the first prototype of such device as well as the details of instrument construction are presented in [19]. The first constraints to consider are the size and geometry of the enclosure in which the electronic device is packed. Due to the spherical geometry and simplicity, two solenoid coils are chosen to develop the inductive link. One of the coils presents a diameter slightly larger than the diameter of the sphere to work as a primary coil. The secondary coil is located inside the sphere, which is sealed. The relative position between the two coils is crucial to define the coupling factor k. A slight misalignment between the coils causes the variation in the

$$p = \frac{(R_1+R_S)\left(2R_2R_L + L_2^2\omega^2 + R_L^2(-1+C_2L_2\omega^2)^2 + R_2^2(1+C_2^2R_L^2\omega^2)\right)}{k^2 L_1 L_2 R_L \omega^2} \tag{10}$$

Fig. 13. Prototype of the charger and the sealed measurement device.

coupling factor and, consequently, in the resonance frequency, as shown in Section II. The coupling coefficient k is evaluated by measuring the voltage V_2 (open circuit), when V_1 is supplied by a voltage source, and the inductances of the link coils L_1 and L_2. Finally, one can observe that the tune loss considerably decreases the ability to transfer energy to the load.

A. Power on the Load

The circuit shown in Fig. 8 is used to test different relative positions between primary and secondary coils and for the measurement of the total power delivered to the load. Concerning coil alignment, three situations are considered.

a. The secondary coil is aligned inside the primary coil, and the coupling factor is $k \approx 0.6$.
b. The secondary coil is misaligned inside the primary coil, and the coupling factor is $k \approx 0.3$.
c. The secondary coil is placed in an intermediary position in order to have a coupling factor of $k \approx 0.4$.

These values for the coupling k are evaluated according the relative position of the device inside the charger. Fig. 13 shows the battery charger prototype and the sphere with the secondary coil. One can see the mark on the sphere representing the right position.

Situations *a* and *b* are considered the best and worst relative positions for the secondary coil. The resonant frequency is only a reference point for the laboratory-evaluated prototype in order to illustrate the deviations of the resonant frequency when the coupling factor k changes.

In these experiments (see the circuit of Fig. 8), the load Z_L is a set of resistors. The range of resistors was chosen in order to observe the value of the load (resistive) around the maximum power dissipation. The output voltage V_1 and V_Z, as well as the efficiency (ratio of the power in and the power out) of the circuit, are measured, and the results are shown in Table II. The component values are the same as that used in the simulations presented in Table I: $R_S + R_{L1} = 1\ \Omega$, $R_{L2} = 0.9\ \Omega$, $L_1 = 90\ \mu$H, $L_2 = 68\ \mu$H, $C = 210$ nF, $C_R = 100\ \mu$F, $e_s(t)$ is an ac pulse source ranging from -5 to $+5$ V, and the frequency is fixed for each k.

TABLE II
EXPERIMENTAL VOLTAGES ON THE LOAD BASED ON RESISTIVE LOAD

	Z_L	$V_1(AC)$	$V_Z(DC)$	η (%)
k=0.3 43kHz	6.8Ω	2.3 Vp	0.3 V	7
	47 Ω	3.8 Vp	1.8 V	33
	270 Ω	8.8 Vp	6.6 V	73
	470 Ω	11.3 Vp	9.0 V	75
	1k Ω	14.3 Vp	13.6 V	71
k=0.4 46kHz	6.8Ω	2.5 Vp	0.4 V	9
	47 Ω	4.8 Vp	2.6 V	49
	270 Ω	12.5 Vp	9.6 V	82
	470 Ω	15.2 Vp	13 V	73
	1k Ω	19.6 Vp	17 V	53
k=0.6 52kHz	6,8Ω	2.9 Vp	0.7 V	12
	47 Ω	6.2 Vp	3.7 V	44
	270 Ω	15 Vp	12.2 V	52
	470 Ω	18 Vp	15.5 V	42
	1k Ω	20 Vp	17.3 V	21

Disregarding the possible measurement errors, the experimental results shown in Table II presented the same trend as the simulated results of Table I. Also, from the equivalent circuit of Fig. 5, one can see that the maximum power occurs when the load assumes the same value as the equivalent resistance which represents the parasitic resistors of inductors, capacitor, and power source reflected to the secondary equivalent circuit. The results show that this value of resistance is around 270 Ω for the parameters of the presenting problem.

B. Wireless Tuning

The load voltage and power are sensitive to frequency variations, as shown in Figs. 7, 9, and 10. Also, the resonance frequency is sensitive to the variation of the coupling factor k. Because of the spherical shape of the instrument, it is inevitable that the relative position between the coils of the charger varies each time that the battery is recharged, varying the inductance reflected to the secondary. Therefore, an adaptive control for fine-tuning the resonance frequency of the secondary coil circuit is suitable. This is done using a wireless communication link between the control and the power system. This wireless link is already available, previously used to collect data from the inside of the instrument.

Concerning platforms that include microcontroller unit (MCU) and radio in the same chip, there are several options, among which is Freescale's MC1322X. This platform includes an ARM 7 MCU and an IEEE 802.15.4 radio, aside from standard peripherals such as a 12-b Analog-to-Digital Converter with multiple inputs. Since such platform has been used in the development of the measuring device, it is suitable for the application of the battery charger. Thus, the

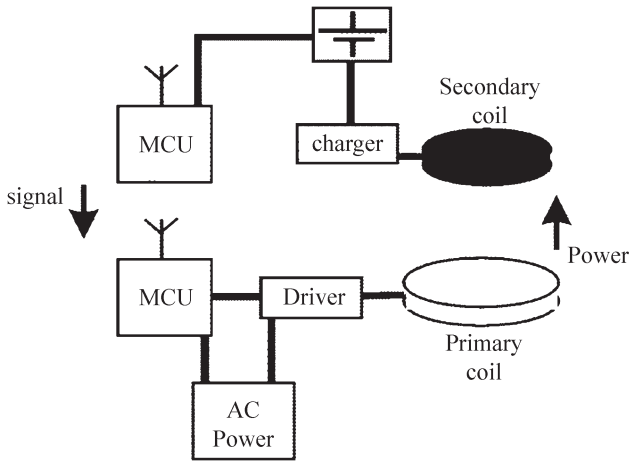

Fig. 14. Block diagram of the charger.

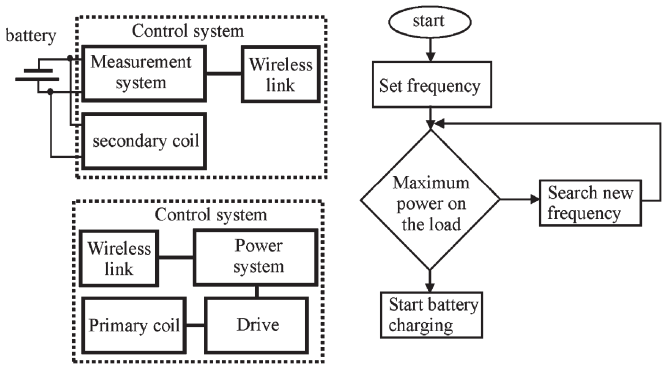

Fig. 15. Block diagram of the charger with wireless communication.

MCU in the measuring device monitors the battery and communicates with the MCU that controls and adjusts the frequency in the charger base, working in the primary coil (see Fig. 14).

In the software side, the MCU of the primary coil initializes the communication link with the MCU of the secondary coil. Thus, the control system on the primary side starts a scan frequency synchronized with the measurements of power in the load carried by the control system on the secondary side. At each frequency point, a measurement of power is performed on the secondary side. This measurement is sent by the wireless link to the primary and compared with the previous data. The algorithm scans for the optimum point, adopts it as the resonance frequency, and starts charging the battery. Fig. 15 illustrates the described wireless loop.

IV. Conclusion

This paper presents the analysis of an inductive power transfer link composed by two coils, used for charging a battery of a portable electronic device that monitors variables associated with the fruit transportation. The primary coil is connected to a power source controlled by an MCU, which, among other features, has a wireless communication module to collect data from the instrument. The secondary coil is connected to the battery charging circuit in which the current and voltage are monitored. This monitoring is made by another MCU that controls the measuring device and communicates with the base.

The inductive link analysis showed that a series resonant capacitor in the primary coil can increase the power at this side. Also, a resonant capacitor on the secondary coil can optimize power on the load. In addition, this study showed that the efficiency of the inductive link is also influenced by the variation of the coupling factor and, consequently, by a compensation capacitor. Thus, in general, the choice of circuit parameters that make up the link can be designed to obtain optimal values of efficiency.

The analysis also showed that the coupling factor k influences the resonance frequency of the circuit, deteriorating the performance of the inductive link. Although there is a visual mark on the device to ensure a perfect fit in the battery charger, there is often a slight misalignment between the coils, making the coupling factor vary from 0.3 to 0.6. The simulations and experimental measurements confirmed that the resonant frequency can range from around 43 to 52 kHz with the coupling factor ranging from 0.3 to 0.6. Also, when the coupling factor is less than 0.1, the variations of k are insignificant to the resonant frequency. Therefore, a closed-loop system was developed in order to monitor the power delivered from the primary to a secondary side of an inductive power transfer with wireless tuning during the battery charging process. The MCU that monitors the loader circuit in the device communicates with the MCU that controls the primary coil driver when the charging process starts. The MCU in the ac power base starts the frequency scanning, searching for the value where the maximal power is delivered to the battery charging circuit. This point is assumed to be the resonance frequency; thus, the battery charge process continues until the full charge is reached.

References

[1] P. Li and R. Bashirullah, "A wireless power interface for rechargeable battery operated medical implants," *IEEE Trans. Circuits Syst. II, Exp. Briefs*, vol. 54, no. 10, pp. 912–916, Oct. 2007.

[2] R. R. Harrison, "Designing efficient inductive power links for implantable devices," in *Proc. IEEE ISCAS*, New Orleans, LA, USA, 2007, pp. 2080–2083.

[3] J. de Boeij, E. Lomonova, J. L. Duarte, and A. J. A. Vandenput, "Contactless power supply for moving sensors and actuators in high-precision mechatronic systems with long-stroke power transfer capability in x-y plane," *Sens. Actuators A, Phys.*, vol. 148, no. 1, pp. 319–328, Nov. 2008.

[4] C.-G. Kim, D.-H. Seo, J.-S. You, J.-H. Park, and B. H. Cho, "Design of a contactless battery charger for cellular phone," *IEEE Trans. Ind. Electron.*, vol. 48, no. 6, pp. 1238–1247, Dec. 2001.

[5] C.-S. Wang, O. H. Stielau, and G. A. Covic, "Design considerations for a contactless electric vehicle battery charger," *IEEE Trans. Ind. Electron.*, vol. 52, no. 5, pp. 1308–1314, Oct. 2005.

[6] T. Bieler, M. Perrottet, V. Nguyen, and Y. Perriard, "Contactless power and information transmission," in *Conf. Rec. IEEE IAS Annu. Meeting*, 2001, vol. 1, pp. 83–88.

[7] C.-J. Chen, T.-H. Chu, C.-L. Lin, and Z.-C. Jou, "A study of loosely coupled coils for wireless power transfer," *IEEE Trans. Circuits Syst. II, Exp. Briefs*, vol. 57, no. 7, pp. 536–540, Jul. 2010.

[8] M. Mark, T. Björninen, L. Ukkonen, L. Sydänheimo, and J. M. Rabaey, "SAR reduction and link optimization for mm-size remotely powered wireless implants using segmented loop antennas," in *Proc. IEEE Topical Conf. BioWireleSS*, Jan. 16–19, 2011, pp. 7–10.

[9] S. Hussmann and A. P. Hu, "A microcomputer controlled ICPT power pick-up and its EMC considerations for moving sensor applications," in *Proc. Int. Conf. Power Syst. Technol.*, Oct. 13–17, 2002, pp. 1011–1015.

[10] J.-U. W. Hsu, A. P. Hu, and A. Swain, "A wireless power pickup based on directional tuning control of magnetic amplifier," *IEEE Trans. Ind. Electron.*, vol. 56, no. 7, pp. 2771–2781, Jul. 2009.
[11] J.-U. W. Hsu, A. P. Hu, and A. Swain, "Fuzzy based directional tuning controller for a wireless power pick-up," in *Proc. IEEE TENCON*, Nov. 19–21, 2008, pp. 1–6.
[12] Y.-H. Chao, J.-J. Shieh, C.-T. Pan, W.-C. Shen, and M.-P. Chen, "A primary-side control strategy for series-parallel loosely coupled inductive power transfer systems," in *Proc. 2nd ICIEA*, May 23–25, 2007, pp. 2322–2327.
[13] G. A. Covic, J. T. Boys, M. L. G. Kissin, and H. G. Lu, "A three-phase inductive power transfer system for roadway-powered vehicles," *IEEE Trans. Ind. Electron.*, vol. 54, no. 6, pp. 3370–3378, Dec. 2007.
[14] C.-S. Wang, O. H. Stielau, and G. A. Covic, "Load models and their application in the design of loosely coupled inductive power transfer systems," in *Proc. Int. Conf. Power Syst. Technol., PowerCon*, Dec. 4–7, 2000, pp. 1053–1058.
[15] J. James, J. T. Boys, and G. A. Covic, "A variable inductor based tuning method for ICPT pickups," in *Proc. 7th IPEC*, Nov. 29–Dec. 2, 2005, pp. 1142–1146.
[16] P. Si, A. P. Hu, S. Malpas, and D. Budgett, "Switching frequency analysis of dynamically detuned ICPT power pick-ups," in *Proc. Int. Conf. Power Syst. Technol., PowerCon*, Oct. 2006, pp. 1–8.
[17] X. Z. Jian and H. Z. Yu, "A novel wireless charging system for movable telephone with printed-circuit-board windings of different structure and shape respectively," in *Proc. ICEMS*, 2007, pp. 1283–1285.
[18] H. Abe, H. Sakamoto, and K. Harada, "A noncontact charger using a resonant converter with parallel capacitor of the secondary coil," *IEEE Trans. Ind. Appl.*, vol. 36, no. 2, pp. 444–451, Mar./Apr. 2000.
[19] I. Muller, R. M. de Brito, C. E. Pereira, and V. Brusamarello, "Load cells in force sensing analysis—Theory and a novel application," *IEEE Instrum. Meas. Mag.*, vol. 13, no. 1, pp. 15–19, Feb. 2010.
[20] I. Muller, R. M. de Brito, and R. J. Bender, "Instrumented sphere for compression analysis," in *Proc. IEEE IIMTC*, 2008, pp. 244–249.
[21] V. J. Brusamarello, Y. B. Blauth, R. Azambuja, and I. Muller, "A study on inductive power transfer with wireless tuning," in *Proc. IEEE IIMT*, Graz, Austria, 2012, pp. 1098–1103.
[22] J. W. Nilsson and S. A. Riedel, *Electric Circuits*, 8th ed. Englewood Cliffs, NJ, USA: Prentice-Hall, 2007.
[23] C. Wang, G. A. Covic, and O. H. Stielau, "Power transfer capability and bifurcation phenomena of loosely coupled inductive power transfer systems," *IEEE Trans. Ind. Electron.*, vol. 51, no. 1, pp. 148–157, Feb. 2004.
[24] P. Wambsganss and D. Huwig, "Inductive power transmission system with stabilized output voltage using local primary and secondary-side control," in *Proc. 14th EPE-PEMC*, 2010, pp. S15-1–S15-8.

Valner J. Brusamarello (M'09) was born in Antônio Prado, Brazil. He received the B.Sc. degree in electrical engineering and the M.Sc. degree in material science from the Universidade Federal do Rio Grande do Sul (UFRGS), Porto Alegre, Brazil, in 1992 and 1996, respectively, and the D.Sc. degree in material science from the Universidade Federal de Santa Catarina, Florianópolis, Brazil, in 2000.

He is currently a Professor with UFRGS, and his main research interests are focused on the area of electronic instrumentation and signal processing for measurement systems.

Yeddo Braga Blauth was born in Rio de Janeiro, Brazil. He received the B.Sc degree in electrical engineering from the Universidade Federal do Rio Grande do Sul (UFRGS), Porto Alegre, Brazil, in 1979 and the M.Sc. degree in power electronics and the D.Sc. degree in electrical engineering from the Universidade Federal de Santa Catarina, Florianópolis, Brazil, in 1988 and 1999, respectively.

Since 1980, he has been working as a Researcher and as a Professor with UFRGS. He has been teaching many different disciplines like electric circuits, basic electronics, and power electronics, and his current research activities include power electronics, electric drives, and instrumentation.

Dr. Blauth is a member of the Brazilian Power Electronics Society (SOBRAEP).

Ricardo de Azambuja (S'12) was born in Brazil in 1978. He received the B.Eng. and M.Sc. degrees in electrical engineering from the Universidade Federal do Rio Grande do Sul, Porto Alegre, Brazil, in 2005 and 2012, respectively, where he is currently working toward the Ph.D. degree in robotics.

From 2007 to 2010, he worked as a Manager on an engineering company.

Ivan Muller (S'08) received the B.Sc. degree in electrical engineering and the M.Sc. degree from the Federal University of Rio Grande do Sul, Brazil, Porto Alegre, Brazil, in 2003 and 2008, respectively, where he is currently working toward the Ph.D. degree in automation systems.

His main research interests are electronic instrumentation and measurement systems, wireless sensor networks, and power electronics.

Fernando Rangel de Sousa (M'03) received the B.Eng. and M.Sc. degrees in electrical engineering from the Federal University of Campina Grande, Campina Grande, Brazil, in 1996 and 2000, respectively, and the Ph.D. degree from the École d'Ingénieurs TELECOM Paristech, Paris, France, in 2004.

From 1996 to 2000, he worked in industry, in consumer electronics companies such as Sharp and Whirlpool. In 2005, he worked at the Federal University of Santa Catarina (UFSC), Florianópolis, Brazil, as a Visiting Professor. From 2006 to 2009, he was with the Federal University of Rio Grande do Norte, Natal, Brazil where was the Head of the Microelectronics and Embedded Systems Laboratory. He is currently with the Electrical Engineering Department, UFSC, where he founded the Radio Frequency Research Group. At UFSC, he is the Counselor of the IEEE student branch. Along the years, he has served as *ad hoc* consultant for federal science and technology funding agencies such as National Counsel of Technological and Scientific Development, and he has consulted for several private and public companies, providing specialized courses and technical and commercial viability studies in the RF field. He also has served as a reviewer for several specialized conferences and journals.

Prof. de Sousa is currently a member of the steering committee of the Brazilian Society of Microelectronics conference, a counselor of the Brazilian Microelectronics Society, and a coordinator of the circuit design activities in the National Institute of Science and Technology on Micro and Nano Technologies.